JOURNAL OF AIRCRAFT
Vol. 29, No. 6, Nov.–Dec. 1992

Assessment of Microburst Models for Downdraft Estimation

Dan D. Vicroy*
NASA Langley Research Center, Hampton, Virginia 23665

NASA has been conducting research in the development of technologies for forward-looking, airborne, wind shear detection systems. Doppler RADAR and LIDAR are two of the technologies being tested to provide this capability. Both measure the Doppler shift from aerosols, raindrops, and other debris in the air to determine the "line-of-sight" relative velocity of the air. An inherent limitation of this type of system is its inability to measure velocities perpendicular to the line-of-sight. This limitation can result in significant underestimation of the magnitude of wind shear hazard. One solution to this line-of-sight limitation of Doppler type sensors, is to use a theoretical or empirical model of a microburst to estimate the perpendicular velocities from the measured line-of-sight values. This article is a summary of an analytical study to assess the effectiveness of three microburst models in estimating the downdraft from horizontal velocity measurements. The article discusses the development of the models and their characteristics. The models are tested at different stages in the life cycle of a microburst.

Nomenclature

d = diameter of vortex ring viscous core, m
$d_{\min}$ = minimum distance from a point (r, z) to a vortex ring filament, m
F = wind shear hazard index
$f(r)$ = empirical model radial shaping function of the horizontal wind velocity, m/s
g = gravitational acceleration, m/s^2
$g(r^2)$ = empirical model radial shaping function of the vertical wind velocity
$p(z)$ = empirical model vertical shaping function of the horizontal wind velocity
$q(z)$ = empirical model vertical shaping function of the vertical wind velocity, m/s
R_v = radius of the primary vortex ring, m
r = radial coordinate (distance from microburst center), m
r_m = radial coordinate of maximum horizontal wind, m
t = time in microburst life cycle, min
u = wind component in the r-direction (tailwind positive), m/s
$\dot{u}$ = rate of change of horizontal wind component, m/s^2
V = true airspeed, m/s
W_{error} = error in vertical wind component estimate, m/s
w = vertical wind component (updraft positive), m/s
w_{model} = model derived vertical wind component, m/s
Z_v = altitude of the primary vortex ring, m
z = vertical coordinate (positive up), m
z_m = altitude of maximum horizontal wind, m
α = empirical model shaping function variable
Γ = circulation strength of vortex ring, m^2/s
ζ = ring vortex viscous core damping factor
λ = empirical model scaling factor, s^{-1}

Received July 23, 1991; presented as Paper 91-2947 at the AIAA Flight Simulation Technologies Conference, New Orleans, LA, Aug. 12–14, 1991; revision received Nov. 1, 1991; accepted for publication Nov. 2, 1991.

*Aerospace Research Engineer, Vehicle Operations Research Branch, MS 156A. Senior Member AIAA.

Introduction

WIND shear is considered by many in the aviation industry to be one of their major safety issues. Numerous accidents and incidents have occurred that were attributed to low-altitude wind shear. These wind shear accidents are most often associated with the convective outflow of thunderstorms known as microbursts. A microburst has a strong localized downdraft, that causes a significant outflow as it impacts the ground. The hazard of a microburst encounter arises from the rapid shift from head-wind to tail-wind as the airplane penetrates the microburst outflow, which reduces the airplane's airspeed. This is accompanied by the downdraft of the microburst that reduces the airplane's rate of climb. The general effect on the airplane is a rapid loss of energy from which it may not have enough altitude, airspeed, or thrust to overcome.

NASA, in a joint effort with the Federal Aviation Administration, has been conducting research in the development of technologies for forward-looking, airborne, wind shear detection systems. Forward-look systems provide the flight crew with awareness of the presence of wind shear with enough time to avoid the affected area or escape from the encounter. A fundamental requirement for such a wind shear detection system is the ability to reliably estimate the magnitude of the wind shear hazard that would be experienced by an airplane if it were to continue along the line-of-sight. Doppler RADAR and LIDAR are two of the technologies being tested to provide this capability. Both measure the Doppler shift from aerosols, rain drops, and other debris in the air to determine the line-of-sight relative velocity of the air. An inherent limitation of this type of system is its inability to measure velocities perpendicular to the line-of-sight. The presence of a microburst can be detected by measuring the divergence of the horizontal velocity profile, yet, the inability to measure the downdraft results in a significant underestimate of the magnitude and spatial extent of the hazard.

One solution to the line-of-sight limitation is to use a theoretical or empirical model of a microburst to estimate the perpendicular velocities from the measured line-of-sight values. This article is a summary of an analytical study to assess the effectiveness of three microburst models in estimating the downdraft from horizontal velocity measurements; it also discusses the development of the models and their characteristics. The models are tested at different points in the life cycle of a microburst.

This article will first introduce a wind shear hazard index known as the "F-factor" to establish the accuracy with which the downdraft needs to be determined. The microburst sim-

ulation database against which the downdraft models will be evaluated will then be introduced. This will be followed by a description of the three microburst downdraft models and the method of analysis. The analysis results will then be presented, followed by the concluding remarks.

Wind Shear Hazard Index

The magnitude of the hazard posed by a microburst to an airplane can be expressed in terms of the F-factor.[1] The F-factor is a hazard index that represents the rate of specific energy loss due to wind shear. For straight and level flight the F-factor can be expressed as

$$F = (\dot{u}/g) - (w/V) \tag{1}$$

Positive values of F indicate a performance-decreasing situation, and conversely, negative values indicate a performance-increasing condition. The F-factor is directly related to the climb gradient or rate-of-climb capability of the airplane. For example, an F value of 0.2 would indicate a loss in climb gradient capability of 0.2 rad (11.5 deg). If an airplane had a maximum climb angle capability of 10 deg, it would be unable to maintain level flight in that wind shear environment. An average F value of 0.1 or greater, extending over a range of 1 km or more, is considered hazardous to landing or departing airplanes.[1]

As mentioned in the introduction, the Doppler-type wind shear sensors can only measure the line-of-sight divergence of the wind and therefore can only determine the first term of the F-factor equation ($\dot{u}/g$). The inability to determine the second term of the equation results in a significant underestimate of magnitude of the microburst hazard. For landing or departing airplanes at low altitude, the vertical component of F can exceed half the total F-factor. If the error in the computed F-factor is required to be less than 10% of the hazard alert threshold, then the downdraft must be known to within 1 m/s (for typical approach to landing airspeeds).

Microburst Simulation Model

The data upon which the various downdraft models were evaluated was generated with the terminal area simulation system (TASS) high-fidelity microburst simulation model. TASS is a time-dependent, multidimensional, nonhydrostatic, numerical cloud model that has been used extensively in the study of microbursts.[2,3] The model is initiated with the observed environmental conditions existing prior to microburst development and outputs a three-dimensional time history of radar reflectivity, winds, temperature, pressure, water vapor, rainwater, snow, hail, and cloud water. The model has been validated against both ground-based and airborne measurements.[3,4] Three-dimensional data can be generated at horizontal grid resolutions of 200 m. Axisymmetric data can be generated at grid resolutions as fine as 20 m. Although TASS is much too complex to be useful as a downdraft estimation model, it is very useful for generating the database necessary to evaluate such models.

The microburst simulation database used in this paper was axisymmetric with a 20 m grid resolution. The data extended from the microburst core to 4000 m radially and from the ground to 600 m vertically. The model was initiated with the atmospheric conditions measured before the August 2, 1985 Dallas-Fort Worth microburst event. Four different times in the microburst simulation were selected, each 2 min apart. Figure 1 shows the wind vector plots for the four times selected. The first was just before the downdraft impacted the ground, which was at 9 min into the microburst simulation. The second was just after the downdraft hit the ground and began to spread out, which was about the time of maximum horizontal shear. The third was at a point when the outflow vortex ring was well-defined, and the last, near the end of the life cycle.

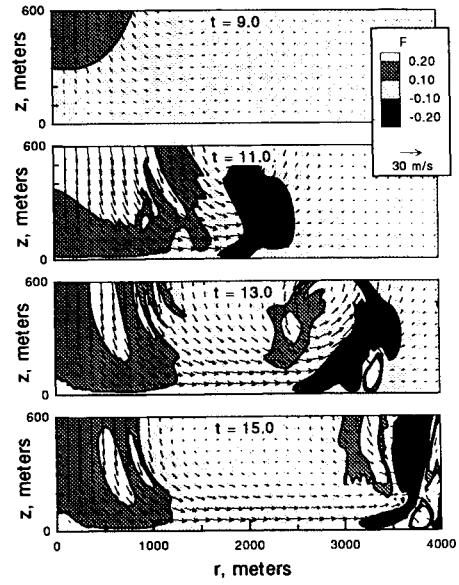

Fig. 1 Wind vectors and F-factor contours of the microburst simulation at four times (t = 9, 11, 13, and 15 min).

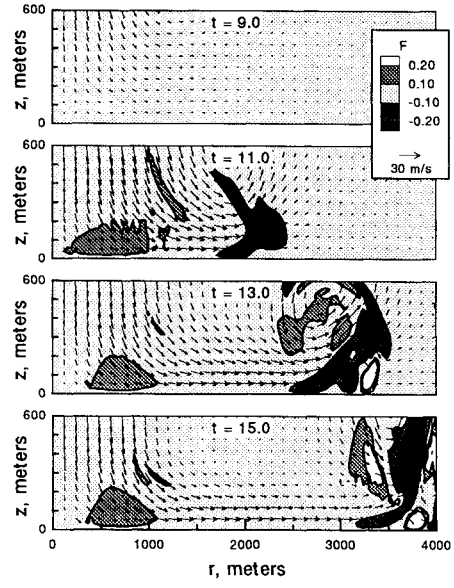

Fig. 2 F-factor contours computed without vertical winds.

Contour plots of F-factor for an airplane flying level at 130 kt are also shown in Fig. 1. Figure 2 shows the same data with the F-factor contours computed without the vertical winds. The magnitude and spatial extent of the detectable hazard is clearly diminished. This further illustrates the need for some means of determining the magnitude of the downdraft.

Microburst Downdraft Models

Three downdraft models were developed for estimating the vertical winds of a microburst from radial wind measurements. The three models represent different levels of sophistication. A description of the three models follows.

Linear Model

The "linear model" is the simplest of the three models tested. It is based primarily on the principle of conservation of mass, that can be expressed in cylindrical coordinates as

$$\frac{\partial u}{\partial r} + \frac{u}{r} + \frac{\partial w}{\partial z} = 0 \tag{2}$$

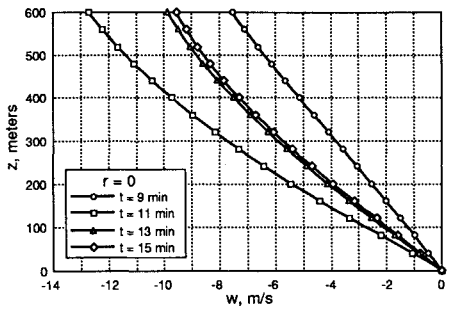

Fig. 3 Vertical wind variation with altitude at the center of the microburst (t = 9, 11, 13, and 15 min).

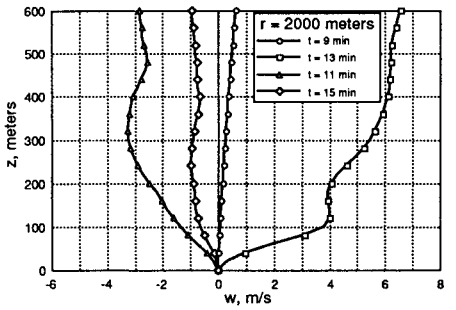

Fig. 4 Vertical wind variation with altitude at a radius of 2000 m (t = 9, 11, 13, and 15 min).

Since the first two terms of the equation can be obtained from the radial velocity measurement, the vertical gradient of the vertical wind can be determined. If the vertical wind is assumed to be zero at the ground and vary linearly with altitude (i.e., $\partial w/\partial z$ = constant), then the vertical wind can be computed from

$$w = \frac{\partial w}{\partial z} z = -z\left(\frac{\partial u}{\partial r} + \frac{u}{r}\right) \tag{3}$$

Figure 3 shows how the downdraft at the center of the microburst varies with altitude for each of the four times. The assumption of linearity is reasonable near the center, particularly at altitudes below 400 m. At higher altitudes the linearity assumption begins to break down. Figure 4 shows the vertical variation of the downdraft at a radius of 2000 m; the linearity assumption is not nearly as valid at this location. This is primarily due to the outflow vortex ring. For the 11 min case, the outflow vortex core was at a radius of about 1800 m, resulting in updrafts at the 2000 m radius. For the 13 min case, the vortex core was beyond the 2000 m radius, resulting in increased local downdraft. The degree to which these nonlinearities introduce errors into the downdraft calculation will be determined in the analysis.

Empirical Model

As the name implies, this model is based on measurements of several microburst events. The empirical model is a modified version of a microburst simulation model developed by Oseguera and Bowles[5] for research in wind shear escape procedures. The changes made to the Oseguera/Bowles' model are discussed in detail in Ref. 6. The empirical model is an axisymmetric, steady-state model that uses shaping functions to satisfy the mass continuity equation and simulate boundary-layer effects.

The mass continuity equation (Eq. (2)) can be satisfied by solutions of the form

$$u = f(r)p(z) \tag{4}$$

$$w = g(r^2)q(z) \tag{5}$$

provided

$$\frac{\partial[rf(r)]}{\partial r^2} = \frac{\lambda}{2} g(r^2) \tag{6}$$

$$\frac{\partial q(z)}{\partial z} = -\lambda p(z) \tag{7}$$

The characteristic shape of the radial shaping functions is shown in Fig. 5. Figures 6 and 7 show the radial profiles of the horizontal and vertical winds from the TASS simulation data at an altitude of 200 m. The shaping functions are used to approximate the characteristic profile of the microburst winds. The shaping functions appear to compare well with

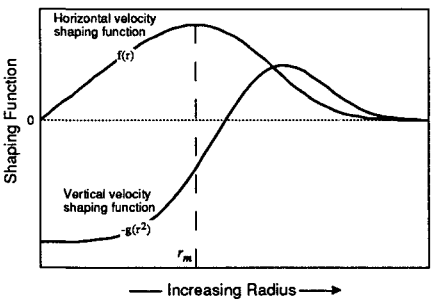

Fig. 5 Characteristic variation of radial-shaping functions.

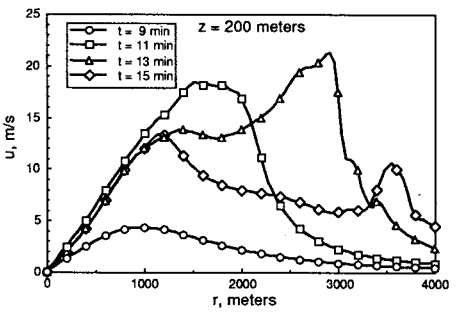

Fig. 6 Radial variation of the horizontal wind at an altitude of 200 m (t = 9, 11, 13, and 15 min).

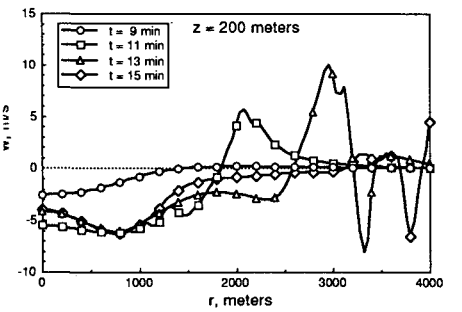

Fig. 7 Radial variation of the vertical wind at an altitude of 200 m (t = 9, 11, 13, and 15 min).

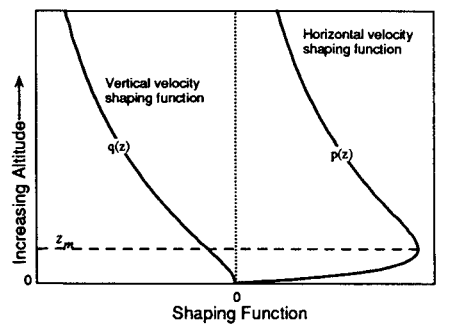

Fig. 8 Characteristic variation of vertical-shaping functions.

the simulation profiles the first two times; but, the radial profiles at the latter times show significant variation due to the outflow vortex ring. As with the linear model, these outflow vortex aberrations may introduce significant errors into the downdraft estimate.

The vertical shaping functions are shown in Fig. 8. Again, the shaping functions compare well with the simulation data shown in Fig. 3, but not in the area of the outflow vortex, as shown in Fig. 4.

The equations for the shaping functions are

$$f(r) = \frac{\lambda r}{2} \exp\left[\frac{2 - (r^2/r_m^2)^\alpha}{2\alpha}\right] \tag{8}$$

$$g(r^2) = \left[1 - \frac{1}{2}\left(\frac{r^2}{r_m^2}\right)^\alpha\right] \exp\left[\frac{2-(r^2/r_m^2)^\alpha}{2\alpha}\right] \tag{9}$$

$$p(z) = \exp\left[c_1\left(\frac{z}{z_m}\right)\right] - \exp\left[c_2\left(\frac{z}{z_m}\right)\right] \tag{10}$$

$$q(z) = -\lambda\left(\frac{z_m}{c_1}\left\{\exp\left[c_1\left(\frac{z}{z_m}\right)\right] - 1\right\} - \frac{z_m}{c_2}\left\{\exp\left[c_2\left(\frac{z}{z_m}\right)\right] - 1\right\}\right) \tag{11}$$

with

$$c_1 = -0.15 \tag{12}$$

$$c_2 = -3.2175 \tag{13}$$

These shaping functions yield the following equations for the horizontal and vertical winds:

$$u = \frac{\lambda r}{2}\left\{\exp\left[c_1\left(\frac{z}{z_m}\right)\right] - \exp\left[c_2\left(\frac{z}{z_m}\right)\right]\right\} \cdot \exp\left[\frac{2 - (r^2/r_m^2)^\alpha}{2\alpha}\right] \tag{14}$$

$$w = -\lambda\left(\frac{z_m}{c_1}\left\{\exp\left[c_1\left(\frac{z}{z_m}\right)\right] - 1\right\} - \frac{z_m}{c_2}\left\{\exp\left[c_2\left(\frac{z}{z_m}\right)\right] - 1\right\}\right) \cdot \left[1 - \frac{1}{2}\left(\frac{r^2}{r_m^2}\right)^\alpha\right] \exp\left[\frac{2 - (r^2/r_m^2)^\alpha}{2\alpha}\right] \tag{15}$$

The empirical model is fully defined through four model variables: the radius and altitude of the maximum horizontal wind (r_m and z_m, respectively), a shaping function variable (α), and a scale factor (λ).

Ring-Vortex Model

The ring-vortex model is a theoretically derived model, based on the assumption that the flowfield generated by a vortex ring, near a flat plate, is similar to that of a microburst. Ring-vortex models have been used in the past as a simple method to simulate microbursts.[7–9] Models using multiple ring-vorticies have shown good correlation with airborne measured microburst winds.[8]

The ring-vortex model has a primary vortex ring located above the ground and a mirror image ring located equidistant below the ground. The mirror image ring is used to satisfy the no-flow through the ground boundary condition. Figure 9 shows the ring-vortex model and the variables that define it. The ring-vortex model is defined by four model variables; the radius and altitude of the primary vortex ring (R_v and Z_v, respectively), the diameter of the viscous core (d), and the circulation strength (Γ).

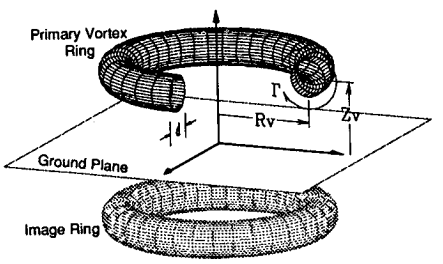

Fig. 9 Ring-vortex model.

The derivation of the velocity equations for the ring-vortex model is discussed in detail in Refs. 7 and 8 and will be omitted here for brevity. The ring-vortex velocity equations are

$$u = \frac{-\Gamma}{2\pi r}\left[\frac{ac(d_1 - d_2)^4(z - Z_v)}{\sqrt{d_1^3 d_2^3}(d_1 + d_2)^2\left(b + \frac{2c\sqrt{d_1 d_2}}{d_1 + d_2}\right)^2} + \frac{3a(d_1 - d_2)^2(z - Z_v)}{d_1 d_2(d_1 + d_2)\left(b + \frac{2c\sqrt{d_1 d_2}}{d_1 + d_2}\right)} - \frac{ac(d_3 - d_4)^4(z + Z_v)}{\sqrt{d_3^3 d_4^3}(d_3 + d_4)^2\left(b + \frac{2c\sqrt{d_3 d_4}}{d_3 + d_4}\right)^2} - \frac{3a(d_3 - d_4)^2(z + Z_v)}{d_3 d_4(d_3 + d_4)\left(b + \frac{2c\sqrt{d_3 d_4}}{d_3 + d_4}\right)}\right] \tag{16}$$

$$w = \frac{-\Gamma}{2\pi r}\left\{\frac{ac(d_1 - d_2)^3[d_1^2(r + R_v) - d_2^2(r - R_v)]}{\sqrt{d_1^3 d_2^3}(d_1 + d_2)^3\left(b + \frac{2c\sqrt{d_1 d_2}}{d_1 + d_2}\right)^2} + \frac{a(d_1 - d_2)[3d_1^2(r + R_v) + 2d_1 d_2 R_v - 3d_2^2(r - R_v)]}{d_1 d_2(d_1 + d_2)^2\left(b + \frac{2c\sqrt{d_1 d_2}}{d_1 + d_2}\right)} - \frac{ac(d_3 - d_4)^3[d_3^2(r + R_v) - d_4^2(r - R_v)]}{\sqrt{d_3^3 d_4^3}(d_3 + d_4)^3\left(b + \frac{2c\sqrt{d_3 d_4}}{d_3 + d_4}\right)^2} - \frac{a(d_3 - d_4)[3d_3^2(r + R_v) + 2d_3 d_4 R_v - 3d_4^2(r - R_v)]}{d_3 d_4(d_3 + d_4)^2\left(b + \frac{2c\sqrt{d_3 d_4}}{d_3 + d_4}\right)}\right\} \tag{17}$$

where

$$d_1 = \sqrt{(r - R_v)^2 + (z - Z_v)^2} \tag{18}$$

$$d_2 = \sqrt{(r + R_v)^2 + (z - Z_v)^2} \tag{19}$$

$$d_3 = \sqrt{(r - R_v)^2 + (z + Z_v)^2} \tag{20}$$

$$d_4 = \sqrt{(r + R_v)^2 + (z + Z_v)^2} \tag{21}$$

$$a = 0.788 \tag{22}$$

$$b = 0.25 \tag{23}$$

$$c = 0.75 \tag{24}$$

The ring-vortex model has singularities along the vertical axis and the vortex core. The singularity along the vertical axis is removed by setting the velocities equal to the limit solution

$$\text{for } r = 0 \begin{cases} u = 0 \\ w = \dfrac{\Gamma R_v^2}{2}\left(1/d_2^3 - 1/d_4^3\right) \end{cases} \tag{25}$$

The singularity at the vortex core is eliminated by multiplying the velocities by a vicious core damping factor (ζ). The viscous core damping factor is the same as in Ref. 8.

$$\zeta = 1 - \exp\left\{\frac{-(d_{\min}/R_v)^2}{\left[k_1\left(\frac{d}{R_v}\right) + k_2\left(\frac{d}{R_v}\right)^2 + k_3\left(\frac{d}{R_v}\right)^3\right]^2}\right\} \tag{26}$$

where $d_{\min}$ is the minimum of d_1 and d_2; and

$$k_1 = 0.4215 \tag{27}$$

$$k_2 = 0.0822 \tag{28}$$

$$k_3 = -0.0969 \tag{29}$$

Method of Analysis

The objective of the downdraft models is to compute the radial distribution of the vertical wind, as shown in Fig. 7, from the radial distribution of the horizontal wind, as shown in Fig. 6. The ability of each of these models to meet this objective was determined by computing the radial downdraft profile from the horizontal velocity profile at each altitude, from 0–600 m, in 20 m steps. The mean and standard deviation of the downdraft estimation error was computed at each altitude and over the total altitude range. The error was defined as

$$W_{\text{error}} = w - w_{\text{model}} \tag{30}$$

Each model computed the downdraft in a slightly different manner. The linear model first computed the radial gradient of the horizontal velocity profile ($\partial u/\partial r$) at each point. The vertical velocity component was then computed from Eq. (3).

The empirical model and the ring-vortex model both used a multivariable search to find the values of the model variables that yielded the best fit to the horizontal velocity profile at each altitude. Using those values, the downdraft profile was then computed for that altitude. The empirical model employed a three variable search for r_m, α, and λ (z_m was set equal to 60 m for this study). The ring-vortex model used a four-variable search for R_v, Z_v, d, and Γ.

Analysis Results

The analysis of the results consisted of studying the characteristics of the downdraft profiles generated at several altitudes, summarizing the error statistics, and proposing methods to improve the model performance.

An example of the fit of the empirical and ring-vortex models to the horizontal velocity profile is shown in Fig. 10. Figure 11 shows the resultant downdraft estimate for all three downdraft models. Early analysis of such profiles lead to two modifications of the models that are reflected in Figs. 10 and 11. The first modification involved only the linear model, that was observed to be very sensitive to local variations in the slope of the horizontal velocity profile ($\partial u/\partial r$). To smooth the downdraft oscillations that resulted from this sensitivity, the method of computing $\partial u/\partial r$ was changed. The new method uses a least-squares linear fit of the horizontal velocity profile over a range of 500 m, centered about the point of interest. The previous method used a 2-point central difference scheme, that is equivalent to a least-squares linear fit over a range of 40 m. The larger averaging range smooths the local variations in the slope resulting in a smoother downdraft profile.

The second modification involved only the empirical and ring-vortex models. These models couldn't reproduce the multiple peaks in the horizontal velocity profile, that were generated by the outflow vortex ring. This was particularly evident in the 13 and 15 min cases where the outflow vortex is well defined. Since the models couldn't accurately fit the horizontal velocity profile, the resultant downdraft estimate

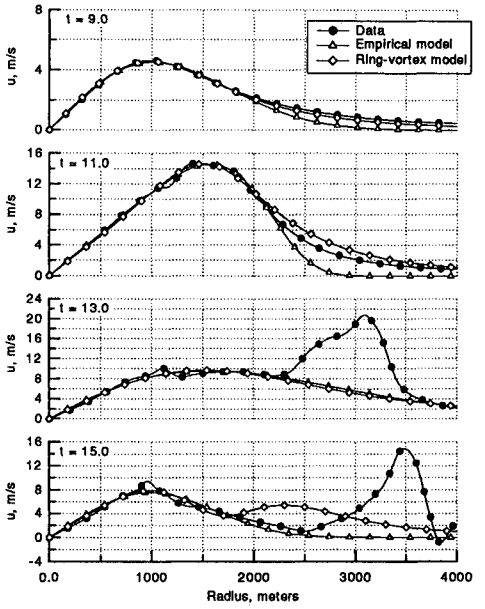

Fig. 10 Fit of the empirical and ring-vortex models to the horizontal velocity profile (z = 300 m).

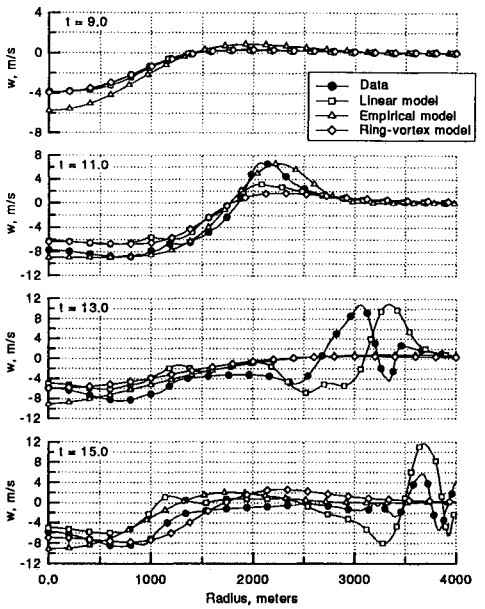

Fig. 11 Comparison to the downdraft profiles generated by the three models (z = 300 m).

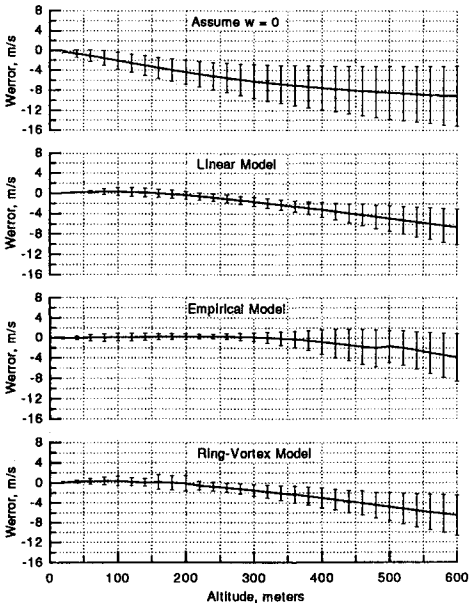

Fig. 12 Mean and standard deviation of the downdraft estimate errors with altitude ($0 \leq r \leq 2000$ m, $t = 11$ min).

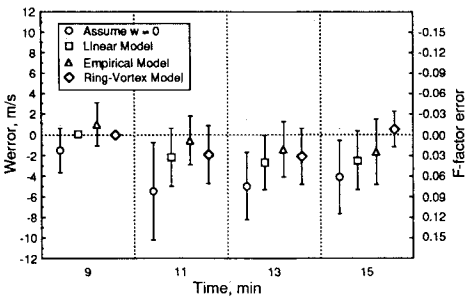

Fig. 13 Total mean and standard deviation of the downdraft and F-factor error ($0 \leq z \leq 600$ m, $0 \leq r \leq 2000$ m).

suffered. The outflow vortex does not contribute to the downdraft over an area large enough to be considered a performance hazard to the airplane. The area in which the downdraft is most significant is near the core of the microburst. The first peak in the horizontal profile is generally associated with the downdraft at the core microburst. The second and third peaks can be associated with the outflow vortex (this is particularly true for this axisymmetric microburst simulation). Asymmetric microbursts may not be as clearly delineated. The empirical and ring-vortex models were modified by limiting the fit of the models to twice the radius of the first peak in the horizontal velocity profile. This improved the model's fit near the core of the microburst, resulting in an improved estimate of the downdraft.

Figure 12 shows the mean and standard deviation of the downdraft estimate errors from the three downdraft models for the 11 min case. Since the downdraft near the core of the microburst is of primary concern, the mean and standard deviation statistics were computed from the core out to a radius of 2000 m. The errors are shown for each altitude at which a downdraft profile was estimated. Also shown in the figure is the error that results from assuming no downdraft ($w = 0$). The errors increased with altitude for all three models; this was expected for the linear model. As previously mentioned, the linearity assumption breaks down at the higher altitudes. The 9, 13, and 15 min cases showed similar trends, but varied in magnitude.

Figure 13 shows the total downdraft error, from 0–600 m altitude and 0–2000 m radius, at each of the four times. Also shown in the figure is the corresponding F-factor error for an airspeed of 130 kt (66.87 m/s). None of the models were able to estimate the downdraft to within the 1 m/s goal. However, all of the models significantly reduced the F-factor error. The ring-vortex and empirical models gave the best overall results. The ring-vortex model provided the best results for the 9 and 15 min cases. The empirical model produced the best results for the 11 and 13 min cases. The 11 min case is near the time of maximum shear and is perhaps the most critical from a hazard perspective. The linear model worked well for all the cases—at altitudes below 200 m—particularly near the core of the microburst.

Concluding Remarks

The primary objective of this study was to assess the effectiveness of three microburst models in estimating the downdraft from horizontal velocity measurements. Although wind shear exists in many forms, the most common form of hazardous wind shear is associated with microbursts. This study is limited to the downdrafts associated with microbursts.

The results of this study show that any of the three models would improve the hazard estimate generated with the downdraft neglected. The linear model works well for altitudes below 200 m and near the microburst core; above 200 m the errors tend to be amplified. The linear model was the simplest of the three models tested.

The ring-vortex and empirical models gave the best overall results. The ring-vortex model was the most complex, requiring four variables to define the model. The empirical model used three model variables. Both the ring-vortex and the empirical model were adversely affected by the variations in the horizontal velocity profile from the outflow vortex ring. This problem can be partially elevated by limiting the model fit to the region near the core of the microburst, where the most significant part of the downdraft occurs.

To fully assess the potential of these microburst models to estimate the downdraft will require considerable more research. This study was limited to a symmetrical microburst simulation. This was done to simplify the problem and assess the model's potential under ideal conditions. Microbursts are not generally symmetrical. The ability of these models to estimate the downdraft of complex asymmetrical microbursts remains to be seen. There are also considerable onboard computation and system implementation issues that have yet to be addressed.

References

[1]Bowles, R. L., *Reducing Windshear Risk Through Airborne Systems Technology*, 17th Congress of the International Congress of Aeronautical Sciences, Stockholm, Sweden, Sept. 1990.

[2]Proctor, F. H., *The Terminal Area Simulation System. Volume I: Theoretical Formulation*, NASA CR-4046, April 1987.

[3]Proctor, F. H., *The Terminal Area Simulation System. Volume II: Verification Cases*, NASA CR-4047, April 1987.

[4]Proctor, F. H., and Bowles, R. L., "Investigation of the Denver 11 July 1988 Microburst Storm with the Three-Dimensional NASA-Langley Windshear Model." *Windshear Case Study: Denver, Colorado, July 11, 1988*, DOT/FAA/DS-89/19, 1989.

[5]Oseguera, R. M., and Bowles, R. L., "A Simple, Analytic 3-Dimensional Downburst Model Based on Boundary Layer Stagnation Flow." NASA TM-100632, July 1988.

[6]Vicroy, D. D., "A Simple, Analytical, Axisymmetric Microburst Model for Downdraft Estimation." NASA TM-104053, DOT/FAA/RD-91/10, Feb. 1991.

[7]Ivan, M., "A Ring-Vortex Downburst Model for Flight Simulations." *Journal of Aircraft*, Vol. 23, No. 3, 1986, pp. 232–236.

[8]Schultz, T. A., "A Multiple Vortex Ring Model of the DFW Microburst." *Journal of Aircraft*, Vol. 27, No. 2, 1990, pp. 163–168.

[9]Zhao, Y., and Bryson, A., "A Simplified Ring-Vortex Downburst Model." AIAA Paper 90-0580, Jan. 1990.